Natural tetramic acids elicit multiple inhibitory actions against mitochondrial machineries presiding over oxidative phosphorylation

Yufu Unten[†], Masatoshi Murai[†]*, Katsuyuki Sakai[‡,1], Yukihiro Asami[‡,#], Takenori Yamamoto[§], Takahiro Masuya[†], and Hideto Miyoshi[†]

Running title: Multiple actions of tetramic acids on mitochondria

[†]Division of Applied Life Sciences, Graduate School of Agriculture, Kyoto University, Kyoto 606-8502, [‡]Graduate School of Infection Control Sciences and [#] Ōmura Satoshi Memorial Institute, Kitasato University, Tokyo 108-8641, and [§]Division of Molecular Target and Gene Therapy Production, National Institute of Health Sciences, Kanagawa 210-9501, Japan.

* To whom correspondence should be addressed: Masatoshi Murai, Division of Applied Life Sciences, Graduate School of Agriculture, Kyoto University, Kyoto 606-8502, Japan, Tel: (+81)-75-753-6406; E-mail: murai.masatoshi.5s@kyoto-u.ac.jp

[1]Present address: Natural Product Biosynthesis Unit, Natural Product Biosynthesis Research Unit, RIKEN Centre for Sustainable Resource Science, Saitama 351-0198, Japan

ABSTRACT

The mitochondrial machineries presiding over ATP synthesis via oxidative phosphorylation are promising druggable targets. Fusaramin, a 3-acyl tetramic acid isolated from *Fusarium concentricum* FKI-7550, is an inhibitor of oxidative phosphorylation in *Saccharomyces cerevisiae* mitochondria, although its target has yet to be identified. Fusaramin significantly interfered with [^{3}H]ADP uptake by yeast mitochondria at the concentration range inhibiting oxidative phosphorylation. A photoreactive fusaramin derivative (pFS-5) specifically labeled voltage-dependent anion channel 1 (VDAC1), which facilitates trafficking of ADP/ATP across the outer mitochondrial membrane. These results strongly suggest that the inhibition of oxidative phosphorylation by fusaramin is predominantly attributable to the impairment of VDAC1 functions. Fusaramin also inhibited F_oF_1-ATP synthase and ubiquinol-cytochrome *c* oxidoreductase (complex III) at concentrations higher than those required for the VDAC inhibition. Considering that other tetramic acid derivatives are reported to inhibit F_oF_1-ATP synthase and complex III, natural tetramic acids were found to elicit multiple inhibitory actions against mitochondrial machineries.

Keywords: tetramic acid, fusaramin, mitochondria, oxidative phosphorylation, VDAC1.

Abbreviations: ADP, adenosine diphosphate; ATP, adenosine triphosphate; CBB, Coomassie Brilliant Blue; IC_{50}, the molar concentration needed to reduce the control electron transfer by 50%; MALDI-TOF MS, matrix-assisted laser desorption/ionization time of flight mass spectrometry; NADH, nicotinamide adenine dinucleotide; NADPH, nicotinamide adenine dinucleotide phosphate; UQ, ubiquinone; SDS-PAGE, sodium dodecyl sulfate-polyacrylamide gel electrophoresis; TAMRA, 6-carboxy-*N,N,N',N'*-tetramethylrhodamine.

INTRODUCTION

The mitochondrial machineries presiding over ATP production through oxidative phosphorylation are promising targets for the development of medicines and agrochemicals. A variety of naturally occurring and synthetic chemicals have been reported to inhibit mitochondrial respiratory enzymes (NADH-ubiquinone oxidoreductase (complex I), succinate-ubiquinone oxidoreductase (complex II), and ubiquinol-cytochrome *c* oxidoreductase (complex III)) and F_oF_1-ATP synthase (*Kita et al. 2007; Weinberg and Chandel 2014; Bald et al. 2017; Murphy 2018*). For example, synthetic agrochemicals such as fenpyroximate and pyridaben were developed as useful acaricides targeting mite mitochondrial complex I (*Clark and Yamaguchi 2002; Murai and Miyoshi 2016*). The anthelmintic compound nafuredin, which was isolated from a culture broth of *Aspergils niger* FT-0554, is an extremely selective inhibitor of complex I in the parasitic helminth *Ascaris suum* (*Ōmura et al. 2001*). Also, many fungicides that target complexes II and III were successfully developed (*Umetsu and Shirai 2020*). As for inhibitors of F_oF_1-ATP synthase, bedaquiline is the first drug to be approved for the treatment of multidrug-resistant *Mycobacterium tuberculosis* (*Andries et al. 2005*).

In contrast to a wide variety of inhibitors targeting mitochondrial respiratory enzymes and F_oF_1-ATP synthase, specific inhibitors of mitochondrial substrate carriers such as ADP/ATP carrier (AAC), phosphate carrier (PiC), and voltage-dependent anion channel (VDAC), which are also essential for oxidative phosphorylation, are highly limited. The consistent use of specific inhibitors of limited targets tends to result in the selection of resistant genotypes and, hence, leads to a rapid decline of the inhibitor's performance. This situation has often been observed in the use of agrochemicals targeting respiratory enzymes (*Avenot and Michailides 2010; Snoeck et al. 2019*). Therefore, both from basic and applied scientific points of view, there is an urgent need to discover new inhibitors targeting the mitochondrial substrate carriers.

Tetramic acid (pyrrolidine-2,4-dione) is a common key structural unit in natural products. To date, numerous natural products containing this unit have been discovered in secondary metabolites from various bioresources such as bacteria, fungi, and marine sponges. For reference, we listed some natural tetramic acids in Table S1, which have largely different chemical frameworks. The tetramic acid moiety is modified by a variety of substructures to form intricate frameworks containing several stereocenters and poly- and macrocyclic skeletons. Because of these complexities, they have received marked interest from synthetic chemists as the targets of total syntheses (*Royles 1995; Mo et al. 2014; Jiang et al. 2020*). The naturally occurring tetramic acids have also attracted a great deal of attention for their broad spectrum of biological activities, including antimicrobial,

antifungal, cytotoxic, and herbicidal activities (*Royles 1995; Mo et al. 2014; Jiang et al. 2020;* see Table S1). Nevertheless, with the exception of tenuazonic acid, which is a phytotoxin isolated from the fungal plant pathogen *Alternaria alternate* that inhibits electron transfer from Q_A to Q_B in photosystem II (*Chen et al. 2007; Chen et al. 2017*), no study has identified the target proteins responsible for the biological activity of natural tetramic acids.

Through a bioassay-guided screening system using multidrug-sensitive *S. cerevisiae* lacking genes of the ATP-binding cassette transporter family (*Sakai et al. 2019*), we recently isolated novel tetramic acid derivatives traminine A and traminine B (Figure 1) from a culture broth of *Fusarium concentricum* FKI-7550 (*Sakai et al. 2021*). Traminine B contains a unique γ-lactam moiety formed by the intramolecular *N*-acylation of pyrrolidine, and traminine A is its ring-opening product. These new tetramic acids inhibited the growth of the yeast on non-fermentable carbon sources such as glycerol, but not that on fermentable carbon sources such as glucose. They inhibited overall ATP production in isolated yeast mitochondria, which was initiated by adding ADP and continuously monitored by detecting ATP released from mitochondria by coupling with ATP-dependent formation of NADPH by hexokinase/glucose-6-phosphate dehydrogenase sequential reactions (*Sakai et al. 2021*). Note that we refer hereafter to this assay as "overall ADP-uptake/ATP-release reactions", which enables us to screen for potential inhibitors of any of the mitochondrial machineries presiding over ATP production via oxidative phosphorylation (i.e, respiratory enzymes, F_oF_1-ATP synthase, and substrate carriers). The above results indicate that traminine A and traminine B inhibit ATP production by oxidative phosphorylation in mitochondria. Based on the results of biochemical characterization using isolated mitochondria, we concluded that the interference with oxidative phosphorylation by traminine A is attributable to the dual inhibition of complex III and F_oF_1-ATPase, whereas that by traminine B is solely due to the inhibition of complex III (*Sakai et al. 2021*).

Using the same yeast screening system and bioresource, we also discovered fusaramin (Figure 1), a tetramic acid derivative composed of β-hydroxyphenylalanine and a polyketide, as an inhibitor of oxidative phosphorylation (*Sakai et al. 2019*). However, fusaramin exhibited no inhibition of respiratory enzymes at a concentration range up to ~3 x IC_{50}, which is the molar concentration required to inhibit overall ADP-uptake/ATP-release reactions by 50% (*Sakai et al. 2019*). These results suggest that the potential target of fusaramin may be the mitochondrial substrate carriers that are essential for oxidative phosphorylation (AAC, PiC, or VDAC); however, we did not investigate its target in the previous work (*Sakai et al. 2019*).

In the present study, we investigated the mechanism of action of fusaramin in *S. cerevisiae* mitochondria through varying biochemical assays and photoaffinity labeling experiments using a synthetic photoreactive derivative (pFS-5, Figure 1). We found that fusaramin binds primarily to VDAC1 and inhibits the overall ADP-uptake/ATP-release reactions at a low concentration range, whereas it also elicits the inhibition of F_oF_1-ATP synthase and complex III activities at further increased concentrations. To the best of our knowledge, fusaramin is the first tetramic acid to be reported that targets mitochondrial VDAC1.

MATERIALS AND METHODS

Materials

Fusaramin, traminine A, and traminine B were the same samples as those used in the previous studies (*Sakai et al. 2019; Sakai et al. 2021*). Carboxyatractyloside (CATR), Ap_5A (P^1,P^5-di(adenosine-5')pentaphosphate), antimycin A, and oligomycin were purchased from Sigma-Aldrich. [^{3}H]ADP was purchased from American Radiolabeled Chemicals. Protein standards (Precision Plus Protein Standards and Precision Plus Protein Dual Xtra Standards) for SDS-PAGE, and hydroxyapatite chromatography (Bio-Gel HT) were obtained from Bio-Rad. The click-iT protein reaction buffer kit and TAMRA-N_3 (Figure S1) were from ThermoFisher Scientific. Other reagents were of analytical grade.

Synthesis of the photoreactive fusaramin derivative pFS-5

The synthetic procedure for the photoreactive fusaramin derivative pFS-5 is described in the supporting information (Scheme S1). All compounds were characterized by ^{1}H- and ^{13}C-NMR spectroscopy and mass spectrometry.

Yeast culture and isolation of mitochondria

The haploid strains of *S. cerevisiae* used in the present study were W303-1B (MATα *ade2-1 leu2-3,112 his3-22,15 trp1-1 ura3-1 can1-100*), *the Δaac* (MATα *ade2-1 leu2-3,112 his3-22,15 trp1-1 ura3-1can1-100 aac1::LEU2 aac2::HIS3*) (*Hashimoto et al. 1999*), and *Δpor1* (MATα *ade2-1 leu2-3,112 his3-22,15 trp1-1 ura3-1 can1-100 por1::HIS3*) (*Yamamoto et al. 2013*). Yeast cells were grown in a 2.0 L Sakaguchi-flask containing 400 mL of semisynthetic lactate medium (2% lactic acid, 0.3% yeast extract, 0.05% glucose, 0.05% $CaCl_2$, 0.05% NaCl, 0.06% $MgCl_2$, 0.1% KH_2PO_4, and 0.1% NH_4Cl) or YPGal medium (1% yeast extract, 2% peptone, and 2% galactose) according to the same conditions as reported previously (*Unten et al. 1999*).

Yeast mitochondria were isolated by digesting cell walls with Zymolyase 20-T (Nacalai-Tesque) followed by careful homogenization and differential centrifugation, as described previously (*Glick et al. 1995; Unten et al. 1999*). The final mitochondrial pellet was resuspended in buffer containing 0.60 M mannitol, 10 mM Tris/HCl (pH 7.4), 0.1 mM EDTA, 0.1% BSA, and protease inhibitor cocktail (for fungal extracts, Sigma-Aldrich). Typically, a total of 1−2 mg of mitochondria was obtained from 800 mL of culture (400 mL x 2 flasks). Protein concentrations were determined using the BCA Protein Assay Kit (Thermo Fisher Scientific) with BSA as the standard.

Measurement of overall ADP-uptake/ATP-release reactions

The measurement of ADP-uptake/ATP-release reactions in isolated yeast mitochondria was conducted as described previously (*Lousa et al. 2002; Unten et al. 1999*). Freshly isolated mitochondria (50 μg of proteins/mL) were suspended in 2.5 mL of reaction buffer (0.60 M mannitol, 0.10 mM EGTA, 2.0 mM $MgCl_2$, 10 mM KP_i, 5.0 mM α-ketoglutarate, and 10 mM Tris-HCl, pH 7.4) at 30˚C in the presence of an ATP-detecting system (2.5 mM glucose, hexokinase (1.7 E.U.), glucose-6-phosphate dehydrogenase (0.85 E.U.), 0.20 mM $NADP^+$, and 10 μM Ap_5A (a specific inhibitor of mitochondrial adenylate kinase)). The addition of ADP (100 μM) started the exchange reaction with ATP that was synthesized in the mitochondrial matrix. The formation of NADPH, which is proportional to ATP efflux, was monitored spectrophotometrically for 10 min at 340 nm (ε = 6.2 mM^{-1} cm^{-1}) with Shimadzu UV-3000.

Measurement of [^{3}H]ADP uptake by yeast mitochondria

The [^{3}H]ADP uptake by isolated mitochondria was measured as reported previously (*Hashimoto et al. 1999, Unten et al. 2019*). In a 1.5 mL Eppendorf tube, freshly isolated mitochondria were incubated with a test compound on ice for 5 min in buffer containing 250 mM sucrose, 10 mM Tris/HCl (pH 7.2), and 0.2 mM EDTA. The reaction was started by the addition of [^{3}H]ADP (40 μM, 1.9 GBq/mmol) to the suspension, followed by incubation on ice for 3 min. Then, the reaction was quenched by the addition of CATR (20 μM), and mitochondria were immediately recovered by centrifugation (15,000 rpm for 5 min at 4˚C). The pellets were resuspended in the same buffer, centrifuged again, solubilized in 2.0% (w/v) SDS (100 μL), and mixed with liquid scintillation cocktail (2 mL, Insta-Gel Plus, PerkinElmer). Radioactivity was assessed using the liquid scintillation counter AccuFLEX LSC-8000 (Hitachi).

Other enzyme assays

For the assays of each respiratory complex, yeast mitochondria were permeabilized by repeated freeze-thawing in 50 mM KPi buffer (pH 7.4) to improve the accessibility of substrates (*Kelso et al. 2001*). NADH-Q_1 oxidoreductase (NDH-2), succinate-cyt. *c* oxidoreductase (complexes II−III), NADH-cyt. *c* oxidoreductase (NDH-2−complex III), and cyt. *c* oxidase (complex IV) activities were measured spectrophotometrically using appropriate electron donor/acceptor pairs (*Unten et al. 2019; Sakai et al. 2021*). Hydrolysis of ATP by F_oF_1-ATP synthase was monitored spectrophotometrically by the enzyme-coupled ATP-regenerating system (*Unten et al. 2019; Sakai et al. 2021*).

Photoaffinity labeling of yeast mitochondria

Yeast mitochondria (1−2 mg of proteins/mL) were resuspended in buffer containing 0.60 M mannitol, 0.10 mM EGTA, 2.0 mM $MgCl_2$, 10 mM KPi, and 10 mM Tris/HCl (pH 7.4), and they were incubated with pFS-5 (1−10 μM) at room temperature for 10 min. Samples were irradiated with a long-wavelength UV lamp (Black Ray model B-100A) on ice for 10 min, positioned 10 cm from the light source (*Murai and Miyoshi 2019*). The labeled mitochondria were collected by centrifugation (15,000 rpm for 5 min at 4˚C), and then subjected to further analysis.

Analysis of the protein labeled by pFS-5

For the separation of mitochondrial carrier proteins, the yeast mitochondria labeled by pFS-5 were solubilized in a buffer containing 10 mM KPi (pH 7.4), 20 mM KCl, 1.0 mM EDTA, protease inhibitor cocktail, and Triton X-100 (at a detergent/protein ratio of 2/1 (w/w)) for 1 h on ice. Then, the sample (approx. 20 μL) was applied to a hydroxyapatite column (Bio-Gel HT, approx. 200 μL bed volume) equilibrated with the same buffer containing 1% (w/v) Triton X-100 (*Yamamoto et al. 2013*). The flow-through fraction was treated with methanol/chloroform, and the precipitate was conjugated with fluorescent TAMRA-N_3 via Cu^+-catalyzed click chemistry (*Unten et al. 2019*) using the Click-iT protein reaction buffer kit (ThermoFisher Scientific). The proteins conjugated with TAMRA-N_3 were resolved on a 15% Laemmli-type SDS gel (*Laemmli 1970*). The migration pattern of fluorescent proteins was visualized by the model FLA-5100 Bioimaging analyzer (Fuji Film, Tokyo, Japan) using a 532 nm light source and LPG (575 nm) filter.

For separation of the respiratory complexes and F_oF_1-ATP synthase, the labeled mitochondria were solubilized with Triton X-100 at a detergent /protein ratio of 2/1 (w/w). The supernatant was separated by Blue Native (BN)-PAGE (*Wittig and Shägger 2005; Wittig et al 2006*) using a 4 to 16% precast gel system (ThermoFisher Scientific) according to the procedures described previously (*Murai et al. 2015*). The bands on the gel were isolated by electroelution using a model 422 Electro-Eluter (Bio-Rad), denatured in 1% (w/v) SDS, conjugated with TAMRA-N_3 via Cu^+-catalyzed click chemistry, and resolved on a 15% Laemmli-type SDS gel, followed by CBB stain and fluorescent gel imaging.

The CBB-stained proteins that correspond to the TAMRA-fluorescence were *"in-gel"* digested with trypsin. The digests were identified by a Bruker Autoflex III Smartbeam instrument (MALDI-TOF/TOF) according to the procedures described previously (*Unten et al 2019*).

RESULTS

Effects of fusaramin on the overall ADP-uptake/ATP-release reactions in isolated S. cerevisiae mitochondria

We first re-examined the inhibition of the overall ADP-uptake/ATP-release reactions by fusaramin using the present *S. cerevisiae* mitochondrial preparations (50 μg of proteins/mL). Fusaramin almost completely inhibited the reactions at concentrations of 5.0–10 μM (100–200 nmol/mg of proteins) with an average IC_{50} value of 1.2 (± 0.25) μM (25 nmol/mg of proteins) (Figure 2). We confirmed that CATR (an inhibitor of the ADP/ATP carrier) and antimycin A (an inhibitor of complex III) completely inhibit the reactions at 208 and 2.08 nmol/mg of proteins, respectively. The inhibitory potency, in terms of the IC_{50} value, of fusaramin was about 1/250 of that of antimycin A (4.8 nM, 0.1 nmol/mg of proteins, *Sakai et al. 2021*). Note that as mitochondrial protein concentrations varied due to the varying assays conducted hereafter, the molarity of the inhibitor in reaction buffer was normalized by the protein concentration (mol inhibitor/mg of proteins) to make comparisons easier.

Effects of fusaramin on the respiratory enzymes and F_oF_1-ATP synthase

Since the mitochondrial respiratory chain provides the driving force for ADP uptake and ATP synthesis by forming a proton electrochemical potential, chemically induced impairments of the respiratory chain or F_oF_1-ATP synthase result in inhibition of the overall ADP-uptake/ATP-release reactions. We previously observed no inhibition of respiratory enzymes or F_oF_1-ATP synthase by fusaramin at concentrations up to ~3 x IC_{50} (*Sakai et al. 2019*). Nevertheless, considering the fact that the other tetramic acid derivatives traminine A and traminine B (Figure 1) inhibit complex III and F_oF_1-ATP synthase activity, respectively (*Sakai et al. 2021*), we cannot exclude the possibility that fusaramin also elicits the inhibition of one or both of these activities at further increased concentrations. Therefore, we need to re-examine the inhibitory effects of fusaramin on each respiratory complex (using appropriate substrate pairs) and F_oF_1-ATP synthase at higher concentrations. Here, we used mitochondrial preparations that were permeabilized by repeated freeze/thawing to improve the accessibility of respiratory substrates.

We tested at three concentrations of fusaramin, 208, 417, and 833 nmol/mg of proteins, which correspond to 8, 16, and 32-fold of the IC_{50} value, respectively, determined for the overall ADP-uptake/ATP-release reactions. Fusaramin exhibits maximum inhibition of the overall ADP-uptake/ATP-release reactions at 208 nmol/mg of proteins, as mentioned above (Figure 2). At 208 and 417 nmol/mg of proteins, fusaramin hardly inhibited respiratory complex activities (NADH-UQ_1 (NDH-2, Figure 3a), NADH-cyt. *c* (NDH-2

and complex III, Figure 3b), and succinate-cyt. *c* (complexes II and III, Figure 3c) oxidoreductase activities, or cyt. *c* oxidase activity (complex IV, Figure 3d)). However, at 833 nmol/mg of proteins, it exhibited slight inhibition of NADH-cyt. *c* and succinate-cyt. *c* oxidoreductase activities (~30 and ~20% inhibition, respectively). Since both enzyme assays include electron flux through complex III, the results indicate that fusaramin inhibits complex III activity at high concentrations. However, it should be noted that the inhibition of complex III by fusaramin is not responsible for its inhibition of the overall ADP-uptake/ATP-release reactions because the latter can be achieved at a lower concentration range (< ~100 nmol/mg of proteins).

On the contrary, fusaramin inhibited F_oF_1-ATP synthase activity (ATP hydrolysis) at all concentrations tested: ~20, ~50, and 60% inhibition at 208, 417, and 833 nmol/mg of proteins, respectively (Figure 3e), which could partly contribute to the interference with the overall ADP-uptake/ATP-release reactions. Taken together, it is likely that inhibition of the overall ADP-uptake/ATP-release reactions by fusaramin is predominantly attributable to the inhibition of ADP uptake by mitochondrial substrate carriers (either AAC or VDAC or both).

Effects of fusaramin on mitochondrial uptake of [^{3}H]ADP

We examined the effects of fusaramin on [^{3}H]ADP uptake by non-respiring yeast mitochondria. Mitochondrial uptake of [^{3}H]ADP in the absence of a respiratory substrate is a well-established assay for mitochondrial substrate carriers including AAC and VDAC (*Hashimoto et al. 1999*). To assure reproducibility of the measurement, we used a 2-fold higher mitochondrial protein concentration in this assay (100 µg of proteins/mL) compared with the overall ADP-uptake/ATP-release assay above (50 µg of proteins/mL).

Fusaramin significantly inhibited [^{3}H]ADP uptake; the incorporated radioactivity decreased to ~40, ~30, and 20% of the control at 100, 200, and 400 nmol/mg of proteins, respectively (Figure 4). We confirmed that CATR inhibits [^{3}H]ADP uptake by ~90% at 100 nmol/mg of proteins. Since fusaramin inhibited [^{3}H]ADP uptake at the same concentration range that inhibits the overall ADP-uptake/ATP-release reactions, it is reasonable to consider that inhibition of the overall ADP-uptake/ATP-release reactions is attributable to the impairment of ADP uptake meditated by mitochondrial substrate carriers, either AAC or VDAC (or both).

Synthesis of a photoreactive fusaramin derivative

To identify the target protein(s) of fusaramin via a photoaffinity labeling technique, we attempted to synthesize photoreactive fusaramin derivatives. In designing the

photoreactive fusaramin derivatives, we prepared a series of derivatives, in which the side chain polyketide is substituted with simpler structures such as *n*-alkyl and prenyl groups (FS-1 and FS-9, respectively, Figure S1) because some structure-activity relationship studies on natural products targeting respiratory enzymes revealed that complicated hydrophobic side chain skeletons are not necessarily essential for their biological activities (*Schnermann et al. 2006; Yoshida et al. 2007; Saimoto et al. 2013*). As expected, fusaramin derivatives possessing *n*-alkyl groups retain the inhibition of the overall ADP-uptake/ATP-release reactions in yeast mitochondria, although their inhibition potencies were slightly weaker than that of natural fusaramin (data not shown).

We synthesized several photoreactive fusaramin derivatives and, consequently, chose pFS-5, which elicited the most potent inhibition of the overall ADP uptake/ATP release reactions, as the test compound (Figure 1). pFS-5 has photolabile phenyldiazirine at the terminal end of the side chain. A terminal alkyne group was introduced into the phenyl ring to allow conjugation of fluorophores via Cu^{+}-catalyzed click chemistry (*Wang et al. 2003*) to visualize the labeled proteins/peptides. We confirmed that pFS-5 inhibits the overall ADP-uptake/ATP-release reactions and [^{3}H]ADP uptake by *S. cerevisiae* mitochondria in a concentration range comparable to that of fusaramin (Figures 2 and 4).

Identification of the mitochondrial substrate carrier labeled by pFS-5

To identify the target carrier of fusaramin, we conducted photoaffinity labeling of *S. cerevisiae* mitochondria using pFS-5. Yeast mitochondria were incubated with 0.5 and 5.0 nmol of pFS-5/mg of proteins (1 and 10 μM at 2.0 mg of proteins/mL), irradiated with a UV lamp. Then, proteins were solubilized with Triton X-100 at a detergent/protein ratio of 2/1 (w/w) and subjected to hydroxyapatite chromatography (*Yamamoto et al. 2013*). The isolated proteins through the chromatography were covalently conjugated with a fluorescent TAMRA-N_3 tag (Figure S1) via Cu^{+}-catalyzed click chemistry to visualize the labeled protein(s), followed by the resolution of proteins on a Laemmli-type SDS gel.

As shown in Figure 5a, two major bands were observed in the CBB-stained SDS gel with apparent molecular weights of ~30 kDa. The upper and lower bands were identified as AAC2 and VDAC1 by MALDI-TOF MS (Table S2), respectively, both of which are major isoforms in *S. cerevisiae*. Although AAC2 and VDAC1 were purified by hydroxyapatite chromatography as an approximately 1:1 mixture (judged by CBB staining), the fluorescence intensity in VDAC1 was much greater than that in AAC2 (~5-fold), indicating that pFS-5 predominantly binds to VDAC1. Identification of the labeled protein was also conducted using a *S. cerevisiae* mutant strain lacking VDAC1 (Δ*por1*) or AAC2 (Δ*aac*, the yeast strain in which intrinsic AAC1 and AAC2 genes were

disrupted). The fluorescence bands of VDAC1 and AAC2 disappeared in Δ*por1* and Δ*aac* strains, respectively (Figure 5b). An excess of fusaramin (100 and 500 molar-fold) suppressed the labeling of VDAC1 by pFS-5, albeit not completely (Figure 5c). The suppressive effect of fusaramin on the labeling of AAC2 was indistinct because the fluorescence intensity of the AAC2 band was inherently weak under the experimental conditions.

We tried to identify the labeled region in VDAC1 by isolating the labeled peptides, which were generated by protease digestion of the labeled VDAC1, and subsequent MS analyses. Unfortunately, we were unable to identify the labeled region because a sufficient amount of the labeled peptides was not obtained. This may be due to the low reaction yields of the photoaffinity labeling as well as intrinsically low binding affinity of fusaramin (pFS-5) to VDAC1. Nevertheless, this is the first report, to the best of our knowledge, revealing that natural tetramic acid binds to VDAC1.

Analysis of the F_oF_1-ATP synthase and complex III labeled by pFS-5

Since fusaramin inhibited F_oF_1-ATP synthase at high concentrations, we tried to identify the subunit(s) to which fusaramin binds. The yeast mitochondria labeled by pFS-5 (10 nmol/mg of proteins) were solubilized with Triton X-100 at a detergent/protein ratio of 2/1 (w/w) and separated on a Blue Native (BN)-gel to provide a monomeric band of F_oF_1-ATP synthase (*Arnold et al. 1998*), which was identified by activity stain using ATP/$Pb(NO_3)_2$ (Figure 6a). The proteins in the band were isolated by electroelution, conjugated with a fluorescent TAMRA-N_3 tag via Cu^+-catalyzed click chemistry, and resolved on a 15% Laemmli-type SDS gel, followed by fluorescent gel imaging, CBB staining, and MS analysis (Figure 6b).

We observed several fluorescent bands as candidates of the labeled subunits, which disappeared in the presence of excess fusaramin (100-fold) during UV irradiation (Figure 6b). MALDI-TOF MS analysis of the major CBB-stained bands indicated that the *b* and *d* subunits (Table S2) were labeled by pFS-5 (indicated by the black arrowheads in Figure 6b). Nevertheless, since the concentration of pFS-5 (0.5 nmol/mg of proteins) used in the labeling experiment is much lower than that required for inhibition of the F_oF_1-ATP synthase activity (> ~80 nmol/mg of proteins, Figure 3e), it remains unclear whether the binding of pFS-5 (or fusaramin) to the subunits is directly responsible for inhibition of the enzyme activity. Note that since fluorescence intensities of the protein bands at ~20 kDa, which are located between the *b* and *d* subunits, markedly changed depending on the experiments, we did not regard this labeling as specific.

Unexpectedly, MALDI-TOF MS analysis revealed that the ~40-kDa protein band labeled by pFS-5 (red arrowhead in Figure 6b) is a Cor1 subunit located in the matrix side of complex III (Table S2). This means that the monomeric F_oF_1-ATPase co-migrates with complex III on the BN gel (*Shägger and Jagow 1991; Arnold et al. 1999*). In this case also, it is unclear whether the binding of pFS-5 (or fusaramin) to this subunit is directly responsible for inhibition of the complex III activity (Figure 3) for the same reason as mentioned above.

DISCUSSION

Natural tetramic acid analogues have attracted great attention because of their diverse biological activities, whereas few studies reported the target proteins responsible for their activities. We previously showed that traminine B (Figure 1a) inhibits oxidative phosphorylation in isolated yeast mitochondria by blocking complex III at a Q_o site and that traminine A (Figure 1a) inhibits both complex III and F_oF_1-ATPase (*Sakai et al. 2021*). The present study demonstrated that fusaramin exhibits multiple inhibitory effects: it inhibits VDAC1 at a low concentration range (< ~200 nmol/mg proteins) but elicits additional inhibition against complex III and F_oF_1-ATP synthase with further increasing concentrations (> ~400 nmol/mg proteins).

Although fusaramin was found to inhibit VDAC1, we did not examine the effects of traminine A and B on the VDAC1 function in the previous study (*Sakai et al. 2021*). To assess whether the inhibition of VDAC1 is a common effect of natural tetramic acids, we examined the effects of traminine A and B on the [^{3}H]ADP uptake by the isolated yeast mitochondria. At a concentration range up to ~3 x IC_{50} of the overall ADP-uptake/ATP-release reactions, traminine A markedly inhibited [^{3}H]ADP uptake, whereas the inhibition by traminine B was partial (by ~20%, Figure S2). It is, therefore, likely that in addition to the inhibition of complex III and F_oF_1-ATP synthase, inhibition of the VDAC1 function is also responsible for interference with oxidative phosphorylation by traminine A and B (*Sakai et al. 2021*). Altogether, inhibition of the VDAC1 function may be a common action among natural tetramic acids, although the binding affinities are different for varying chemical frameworks.

König *et al*. reported the multiple inhibitory effects of equisetin (Table S1), an antibiotic possessing a tetramic acid scaffold produced by *Fusarium equiseti*, on rat liver mitochondria. Equisetin was shown to inhibit uptake of substrate anions such as ATP, phosphate, and succinate (*König et al. 1993*). As this antibiotic did not affect bilayer-reconstituted VDAC1 channel conductance, König *et al*. postulated that the inhibitory effects on the substrate transport are attributed to the multiple inhibitions of mitochondrial carriers that reside in the inner membrane such as AAC, PiC, and dicarboxylate carrier, rather than VDAC1 in the outer membrane (*König et al. 1993*). However, it is generally considered that VDAC1 also regulates the transport of various substrates across the inner membrane, likely at contact sites of the two membranes through interaction with various proteins, including AAC and PiC (*Colombini 2012; Mauze 2017; Shoshan-Barmatz et al. 1017; Margì et al. 1018; Di Rosa et al. 2021*). In light of this, we still cannot exclude the possibility that the binding of equisetin to VDAC1 may affect the transport of substrates across the inner membrane.

VDAC1 situated in the outer mitochondrial membrane serves as a mitochondrial gatekeeper, which facilitates the trafficking of various ions and metabolites between the cytoplasm and mitochondrial intermembrane space (*Colombini 2012; Mauze 2017; Shoshan-Barmatz et al. 1017; Margì et al. 1018; Di Rosa et al. 2021*). Since VDAC1 also plays a key role in mitochondrial permeability transition and mitochondria-meditated apoptosis, it has potential as a promising target for anticancer therapeutics (*Shoshan-Barmatz et al. 1017; Margì et al. 1018*). However, because VDAC1 has a bucket-like structure (19-stranded β-barrel fold) (*Hiller et al. 2008; Bayrhuber et al. 2008; Ujiwal et al. 2008*), it may not possess a ligandable pocket based on the "lock and key" analogy. In this sense, the tetramic acid scaffold is unique and valuable as the pharmacophore required for binding to VDAC1 and, hence, worth further modifying their structures to produce potential lead compounds for new medicines and/or agrochemicals. At the same time, molecular designs to produce tetramic acid derivatives, which elicit highly specific inhibition solely of VDAC1, are challenging from a synthetic chemical point of view. Such efforts are currently underway in our laboratory.

Concerning the 3-acyl tetramic acid scaffold, four keto-enol tautomers, involving two sets of rapidly interconverting internal tautomers, are generally detected in organic solvents (Figure 1b, *Royles 1995; Mo et al. 2014*). The versatile chemical frameworks of the toxophoric moiety of tetramic acids could be responsible for their multiple actions against mitochondrial machineries demonstrated in this study. A survey of the literature revealed similar cases for several natural products. For example, natural polyphenol curcumin analogues, which are represented as an interconverting mixture of the symmetric di-keto and asymmetric β-keto-enol tautomers (Figure S3, *Payton et al. 2007; Gupta et al. 2011; Esatbeyoglu et al. 2012*), elicit various biological activities, which are considered to be due to interactions with different types of target proteins such as inflammatory proteins and kinases (*Gupta et al. 2011*) and Alzheimer's disease-related proteins (*Konno et al. 2014; Okuda et al. 2016; Di Martino et al. 2016*).

ACKNOWLEDGEMENTS

We thank Drs. Takeshi Nakano and Kentaro Ifuku (Division of Integrated Life Science, Graduate School of Biostudies, Kyoto University) for allowing us access to their MALDI-TOF MS (Bruker Autoflex III Smartbeam) and for their helpful advice on the experiments. The experiments involving radioisotope techniques were performed at the Radioisotope Research Center, Kyoto University.

SUPPLEMENTARY MATERIAL

This article contains Figures S1-S3, Tables S1 and S2, and Scheme S1. They are available free of charge via the Internet.

DATA AVAILABILITY

The data underlying this article are available in the article and in its online supplementary material.

AUTHOR CONTRIBUTION

Y.U., M.M., and H.M. designed the research; Y.U, M.M., K.S. performed the research and analyzed the data with Y.A., T.Y., T.M., and H.M.; M.M. and H.M. directed the project and wrote the paper with Y.U.

FUNDING

This work was supported by JSPS KAKENHI (Grant Numbers JP21H02130 to H.M., Grant Number 21J10772 to Y.U. and Grant Number 20K15457 to T.M.) and by ISHIZUE 2021 of Kyoto University Research Development Program (to M.M.).

DISCLOSURE STATEMENT

The authors declare no competing financial interest.

REFERENCES

- Andries K, Verhasselt P, Guillemont J et al. A diarylquinoline drug active on the ATP synthase of *Mycobacterium tuberculosis*. *Science* 2005;**307**:223-227.
- Arnold I, Pfeiffer K, Neupert W et al. ATP synthase of yeast mitochondria, *J Biol Chem* 1999;**274**:36-40.
- Arnold I, Pfeiffer K, Neupert W et al. Yeast mitochondrial F_oF_1-ATP synthase exists as a dimer: identification of three dimer-specific subunits. *EMBO J* 1998;**17**:7170-7178.
- Avenot HF, Michailides TJ. Progress in understanding molecular mechanisms and evolution of resistance to succinate dehydrogenase inhibiting (SDHI) fungicides in phytopathogenic fungi. *Crop Protection* 2010;**29**:643-651.
- Bald D, Villellas C, Lu P et al. Targeting Energy Metabolism in *Mycobacterium tuberculosis*, a new paradigm in antimycobacterial drug discovery. *mBio* 2017;**8**:e00272-17.
- Bayrhuber M, Meins T, Habeck M et al. Structure of the human voltage-dependent anion channel. *Proc Natl Acad USA* 2008;**105**:15370-15375.
- Chen S, Qiang S. Recent advances in tenuazonic acid as a potential herbicide. *Pestic. Biochem Physiol* 2017;**143**:252-257.
- Chen S, Xu X, Dai X, et al. Identification of tenuazonic acid as a novel type of natural photosystem II inhibitor binding in Q_B-site of *Chlamydomonas reinhardtii*. *Biochem Biophys Acta* 2007;**1767**:306-318.
- Clark JM, Yamaguchi I. Scope and status of pesticide resistance. In: Clark JM, Yamaguchi I (Ed). Agrochemical resistance: extent, mechanism, and detection. Washington DC: American Chemical Society, 2002, 1-22.
- Colombini M. VDAC structure, selectivity, and dynamics. *Biochim Biophys Acta* 2012;**1818**:1457−1465.
- Di Martino RM, De Simone A, Andrisano V et al. Versatility of the curcumin scaffold: discovery of potent and balanced dual BACE-1 and GSK-3β Inhibitors. *J Med Chem* 2016;**59**:531-544.
- Di Rosa MC, Guarino F, Nibali SC et al. Voltage-Dependent Anion Selective Channel Isoforms in Yeast: Expression, Structure, and Functions. *Front Physiol* 2021;**12**:675708.

- Esatbeyoglu T, Huebbe P, Ernst IMA et al. Curcumin-from molecule to biological function. *Angew Chem Int Ed* 2012;**51**:5308-5332.
- Glick BS, Pon LA. Isolation of highly purified mitochondria from *Saccharomyces cerevisiae Methods Enzymol* 1995;**260**:213-223.
- Gupta SC, Prasad S, Kim JH. Aggarwal, Multitargeting by curcumin as revealed by molecular interaction studies. *Nat Prod Rep* 2011;**28**:1937-1955.
- Hashimoto M, Shinohara Y, Majima E et al. Expression of the bovine heart mitochondrial ADP/ATP carrier in yeast mitochondria: significantly enhanced expression by replacement of the N-terminal region of the bovine carrier by the corresponding regions of the yeast carriers. *Biochim Biophys Acta (Bioenergetics)* 1999;**1409**;113−124.
- Hiller S, Garces RG, Malia TJ et al. Solution structure of the integral human membrane protein VDAC-1 in detergent micelles. *Science* 2008;**321**:1206-1210.
- Jiang M, Chen S, Li J et al. The biological and chemical diversity of tetramic acid compounds from marine-derived microorganisms. *Mar. Drugs* 2020;**18**:114.
- Kelso GF, Porteous CM, Coulter CV et al. Selective targeting of a redox-active ubiquinone to mitochondria within cells antioxidant and antiapoptotic properties. *J Biol Chem* 2001;**276**:4588-4596.
- Kita K, Shiomi K, Ōmura S. Advances in drug discovery and biochemical studies. *Trends in Parasitol* 2007;**23**:223-229.
- Konno H, Endo H, Ise S et al. Synthesis and evaluation of curcumin derivatives toward an inhibitor of beta-site amyloid precursor protein cleaving enzyme 1. *Bioorg Med Chem Lett* 2014;**15**:685-690.
- König T, Kapus A, Sarkadi B. Effects of equisetin on rat liver mitochondria: evidence for inhibition of substrate anion carriers of the inner membrane. *J Bioenerg Biomembr* 1993;**25**:537-545.
- Laemmli UK. Cleavage of structural proteins during the assembly of the head of bacteriophage T4. *Nature* 1970;**227**:680-685.
- Lousa CDM, Trézéguet V, Dianoux AC, et al. The human mitochondrial ADP/ATP carriers: kinetic properties and biogenesis of wild-type and mutant proteins in the yeast *S. cerevisiae*. *Biochemistry* 2002;**41**:14412-14420.
- Magrì A, Reina S, De Pinto V. VDAC1 as pharmacological target in cancer and neurodegeneration: focus on its role in apoptosis. *Front Chem* 2018;**6**:1−17.

- Mazure NM. VDAC in cancer. *Biochim Biophys Acta (Bioenergetics)* 2017;**1858**:665−673.
- Mo X, Li Q, Ju, J. Naturally occurring tetramic acid products: isolation, structure elucidation and biological activity. *RSC Adv* 2014;**4**:50566-50593.
- Murai M, Miyoshi H Current topics on inhibitors of respiratory complex I. *Biochim Biophys Acta (Bioenergetics)* 2016;**1857**:884-891.
- Murai M, Miyoshi H. Photoaffinity labeling of respiratory complex I in bovine heart submitochondrial particles by photoreactive [^{125}I] amilorides. *Bio Protoc* 2019;**9**: e3349.
- Murai M, Murakami S, Ito T et al. Amilorides bind to the quinone binding pocket of bovine mitochondrial complex I. *Biochemistry* 2015;**54**:2739-2746.
- Murphy MP, Hartley RC. (2018) Mitochondria as a therapeutic target for common pathologies. *Nat Rev Drug Discovery* 2018;**17**:865-886.
- Okuda M, Hijikuro I, Fujita Y et al. Design and synthesis of curcumin derivatives as tau and amyloid β dual aggregation inhibitors. *Bioorg Med Chem Lett* 2016;**26**: 5024-5028.
- Ōmura S, Miyadera H, Ui H et al. Anthelmintic compound, nafuredin, shows selective inhibition of complex I in helminth mitochondria. *Proc Natl Acad Sci USA* 2001;**98**:60–62.
- Payton F, Sandusky P, Alworth WL. NMR study of the solution structure of curcumin. *J Nat Prod* 2007;**70**:143-146.
- Royles BJL. Naturally occurring tetramic acids: structure, isolation, and synthesis. *Chem Rev* 1995;**95**:1981-2001.
- Saimoto H, Kido Y, Haga Y et al. Pharmacophore identification of ascofuranone, potent inhibitor of cyanide-insensitive alternative oxidase of *Trypanosoma brucei*. *J Biochem* 2013;**153**:267-273.
- Sakai K, Unten Y, Iwatsuki M et al. Fusaramin, an antimitochondrial compound produced by *Fusarium* sp., discovered using multidrug-sensitive *Saccharomyces cerevisiae. J Antibiot* 2019;**72**:645-652.
- Sakai K, Unten Y, Kimishima A et al. Traminines A and B, produced by *Fusarium concentricum*, inhibit oxidative phosphorylation in *Saccharomyces cerevisiae* mitochondria. *J Ind Microbiol Biotechnol (DOI: 10.1093/jimb/kuab051)*

- Schnermann MJ, Romero FA, Hwang I et al. Total synthesis of piericidin A1 and B1 and key analogues. *J Am Chem Soc* 2006;**128:11799**-11807.
- Schägger H, von Jagow G. Blue native electrophoresis for isolation of membrane protein complexes in enzymatically active form. *Anal Biochem* 1991;**199**:223-231.
- Shoshan-Barmatz V, Krelin Y, Shteinfer-Kuzmine A et al. Voltage-dependent anion channel 1 as an emerging drug target for novel anti-cancer therapeutics. *Front Oncol* 2017;**7**:1−24.
- Snoeck S, Kurlovs AH, Bajda S et al. (2019) High-resolution QTL mapping in *Tetranychus urticae* reveals acaricide-specific responses and common target-site resistance after selection by different METI-I acaricides. *Insect Biochem Mol Biol* 2019;**110**:19-33.
- Ujwal R, Cascio D, Colletier JP et al. The crystal structure of mouse VDAC1 at 2.3 Å resolution reveals mechanistic insights into metabolite gating. *Proc Natl Acad USA* 2008;**105**;17742-17747.
- Umetsu N, Shirai Y. Development of novel pesticides in the 21st century. *J Pestic Sci* 2020;**45**:54-74.
- Unten Y, Murai M, Yamamoto T et al. Pentenediol-type compounds specifically bind to voltage-dependent anion channel 1 in *Saccharomyces cerevisiae* Mitochondria. *Biochemistry* 2019;**58**:1141-1154.
- Wang Q, Chan TR, Hilgraf R et al. Bioconjugation by copper (I)-catalyzed azide-alkyne [3+2] cycloaddition. *J Am Chem Soc* 2003;**15**:3192–3193.
- Weinberg S, Chandel NS. Targeting mitochondria metabolism for cancer therapy. *Nat Chem Biol* 2014;**11**:9-15.
- Wittig I, Braun HP, Schägger H. Blue native PAGE. *Nat Protoc* 2006;**1**:418-28.
- Wittig I, Schägger H. Advantages and limitations of clear-native PAGE. *Proteomics* 2005;**5**:4338-4346.
- Yamamoto T, Tamaki H, Katsuda C et al. Molecular basis of interactions between mitochondrial proteins and hydroxyapatite in the presence of Triton X-100, as revealed by proteomic and recombinant techniques. *J Chromatogr* 2013;**1301**:169-178.
- Yoshida T, Murai M, Abe M et al. Crucial factors and mode of action of polyene amides as inhibitors for mitochondrial NADH-ubiquinone oxidoreductase (complex I). *Biochemistry* 2007;**46**:10365-10372.

FIGURES AND LEGENDS

Figure 1. Structures of test compounds used in this study.
(a) Structures of tetramic acid derivatives isolated from *Fusarium* sp. FKI-7550: Fusaramin, traminine A, traminine B, and photoreactive pFS-5. (b) Structure of four tautomers of 3-acyltetramic acid (*13*).

Figure 2. Inhibition of the overall ADP-uptake/ATP-release reactions by fusaramin or other compounds.
Isolated yeast mitochondria (50 μg of proteins/mL) were incubated with each inhibitor (208 or 2.08 nmol/mg of proteins each (10 or 0.1 μM)) in a reaction buffer supplemented with an ATP-detecting system (see Experimental Procedures). Overall ADP-uptake/ATP-release reactions were monitored by detecting ATP-release, which is proportional to the formation of NADPH. The average ATP efflux in the absence of inhibitor was 0.27 ± 0.03 μmol ATP/min/mg of proteins. Values show means ± SEM (n = 3-5). The significance of pairwise comparisons with the control was assessed with Dunnett's test. $^{***}P<0.001$.

Figure 3. Effects of fusaramin on the respiratory enzymes and F_oF_1-ATP synthase activities.
a: NADH-UQ_1 oxidoreductase activity (NDH-2), b: NADH-cyt. *c* oxidoreductase activity (NDH2−complex III), c: succinate-cyt. *c* oxidoreductase activity (complexes II−III), d: cyt. *c* oxidase activity (complex IV), e: ATP hydrolysis activity (ATP synthase). Protein concentrations were set to 12 μg/mL for NADH-UQ_1, NADH-cyt. *c*, succinate-cyt. *c*, and cyt. *c* oxidase activities, and 30 μg/mL for ATP hydrolysis activity, respectively. The numbers of the abscissa of the graph indicate the concentrations of fusaramin (nmol/mg of proteins). Values show means ± SEM (n = 3−4). The significance of pairwise comparisons with the control was assessed with Dunnett's test. $^{***}P<0.001$, $^{**}P<0.01$, $^{*}P<0.05$

Figure 4. Inhibition of [^{3}H]ADP uptake by fusaramin and other compounds.
Isolated yeast mitochondria (100 μg of proteins/mL, 500 μL) were incubated with each compound, and then, [^{3}H]ADP (40 μM, 1.9 GBq/mmol) was added to the mitochondrial suspension, followed by incubation on ice for 3 min. [^{3}H]ADP uptake was terminated by the addition of 10 μM CATR, followed by the quantification of radioactivity. The average uptake of [^{3}H]ADP in the absence of inhibitor was 2.57 ± 0.27 ADP nmol /mg of proteins.

The numbers of the abscissa of the graph indicate the concentrations of test compounds (nmol/mg of proteins). Values show means ± SEM (n = 4–8). The significance of pairwise comparisons with the control was assessed with Dunnett's test. $^{***}P<0.001$

Figure 5. Photoaffinity labeling of mitochondrial substrate carrier(s) by pFS-5.
(a) Yeast mitochondria (2.0 mg of proteins/mL) were labeled with pFS-5 (0.50 and 5.0 nmol/mg of proteins) and partially purified by hydroxyapatite chromatography, followed by conjugation with a fluorescent TAMRA-azido tag via Cu^+-catalyzed click chemistry. Proteins were separated on a 15% Laemmli-type SDS gel, and they were subjected to fluorescent gel imaging and CBB staining. The white and black arrowheads indicate AAC2 (36% coverage by MALDI-TOF MS) and VDAC1 (68% coverage), respectively. (b) Yeast mitochondria isolated from wild-type, Δ*por1* mutant, or Δ*aac* mutant *S. cerevisiae* cells (2.0 mg of protein/mL) were labeled by pFS-5 (5.0 nmol/mg of proteins) and partially purified by hydroxyapatite chromatography, followed by conjugation with a fluorescent TAMRA-azido tag via Cu^+-catalyzed click chemistry. The experimental conditions were the same as those in panel A. (c) Competition test between pFS-5 and fusaramin. Yeast mitochondria (2.0 mg of protein/mL) were labeled with pFS-5 (0.5 nmol/mg of proteins) in the presence or absence of fusaramin. The experimental conditions were the same as those in panel A. The fluorescent intensities of TAMRA incorporated into VDAC1 were normalized by the expression level of VDAC1 estimated by CBB stain. Values shows means ± SEM (n = 3-5).

Figure 6. Photoaffinity labeling of F_oF_1-ATP synthase by pFS-5.
(a) Yeast mitochondria (2.0 mg of proteins/mL) were labeled with pFS-5 (0.5 nmol/mg of proteins) and solubilized using a Triton X-100/protein ratio of 2 (g/g). Proteins were separated on a Blue Native gel to provide a monomeric band of F_oF_1-ATP synthase, which was identified by an in-gel ATPase assay using ATP and $Pb(NO_3)_2$ (*Wittig and Shägger 2005*). (b) Competition test between pFS-5 and fusaramin. Yeast mitochondria (2.0 mg of protein/mL) were labeled with pFS-5 (0.5 nmol/mg of proteins) in the presence or absence of fusaramin. The experimental conditions were the same as those in panel A. Monomeric ATP synthase was eluted from a gel strip of BN-PAGE, followed by conjugation with a fluorescent TAMRA-azido tag via Cu^+-catalyzed click chemistry. These subunits were separated on a 15% Laemmli-type SDS gel and subjected to fluorescent gel imaging and CBB staining. The red arrowhead indicates the COR1 subunit of complex III. The black arrowheads indicate subunit *b* (23 kDa) and *d* (19 kDa) of F_oF_1-ATP synthase.

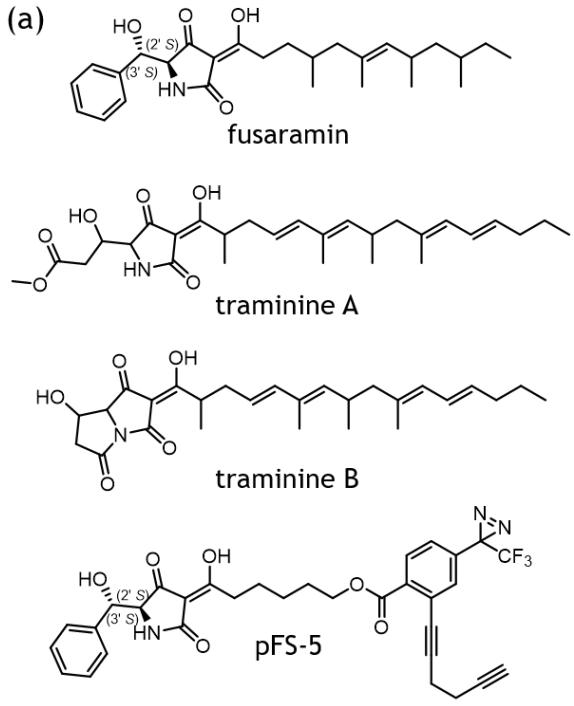

Figure 1

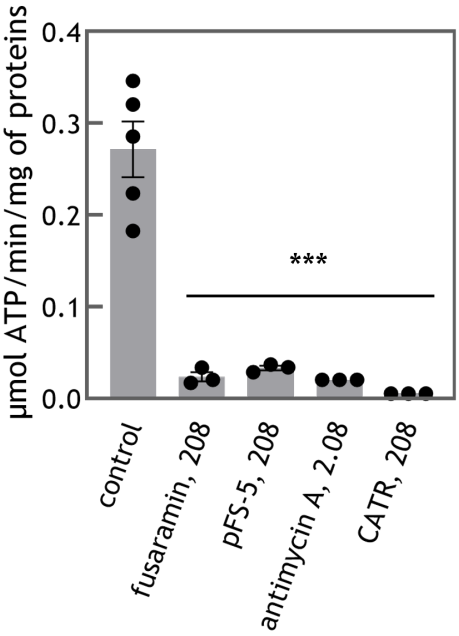
µmol ATP/min/mg of proteins
0.4
0.3
0.2
0.1
0.0
***
control
fusaramin, 208
pFS-5, 208
antimycin A, 2.08
CATR, 208

Figure 2

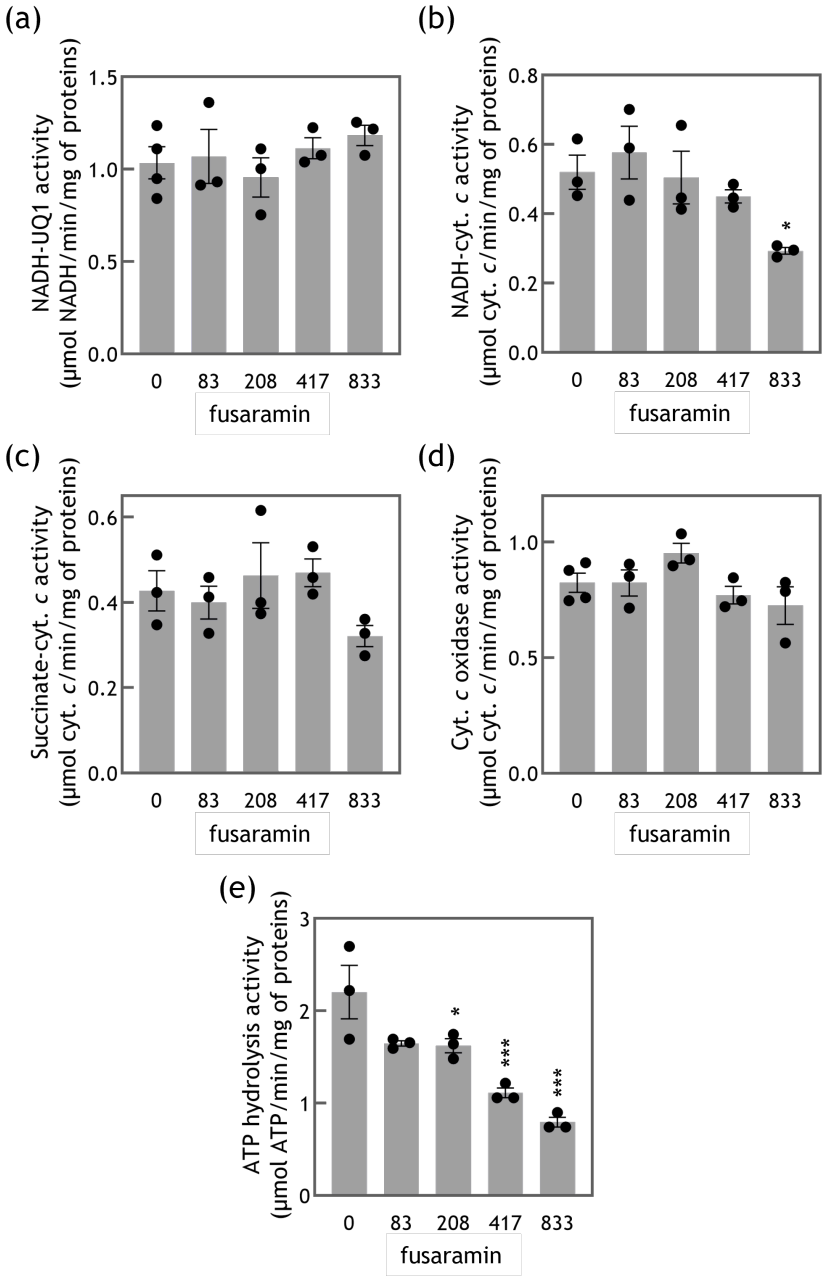
(a)
NADH-UQ1 activity
(µmol NADH/min/mg of proteins)
1.5
1.0
0.5
0.0
0
83
208
417
833
fusaramin
(b)
NADH-cyt. c activity
(µmol cyt. c/min/mg of proteins)
0.8
0.6
0.4
0.2
0.0
*
0
83
208
417
833
fusaramin
(c)
Succinate-cyt. c activity
(µmol cyt. c/min/mg of proteins)
0.6
0.4
0.2
0.0
0
83
208
417
833
fusaramin
(d)
Cyt. c oxidase activity
(µmol cyt. c/min/mg of proteins)
1.0
0.5
0.0
0
83
208
417
833
fusaramin
(e)
ATP hydrolysis activity
(µmol ATP/min/mg of proteins)
3
2
1
0
*
***
***
0
83
208
417
833
fusaramin

Figure 3

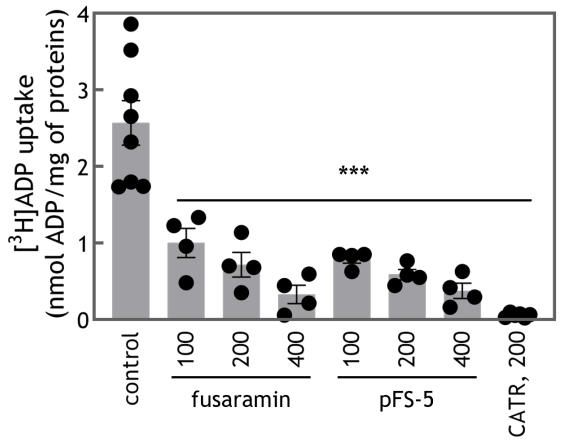
[3H]ADP uptake
(nmol ADP/mg of proteins)
4
3
2
1
0
***
control
100
200
400
100
200
400
fusaramin
pFS-5
CATR, 200

Figure 4

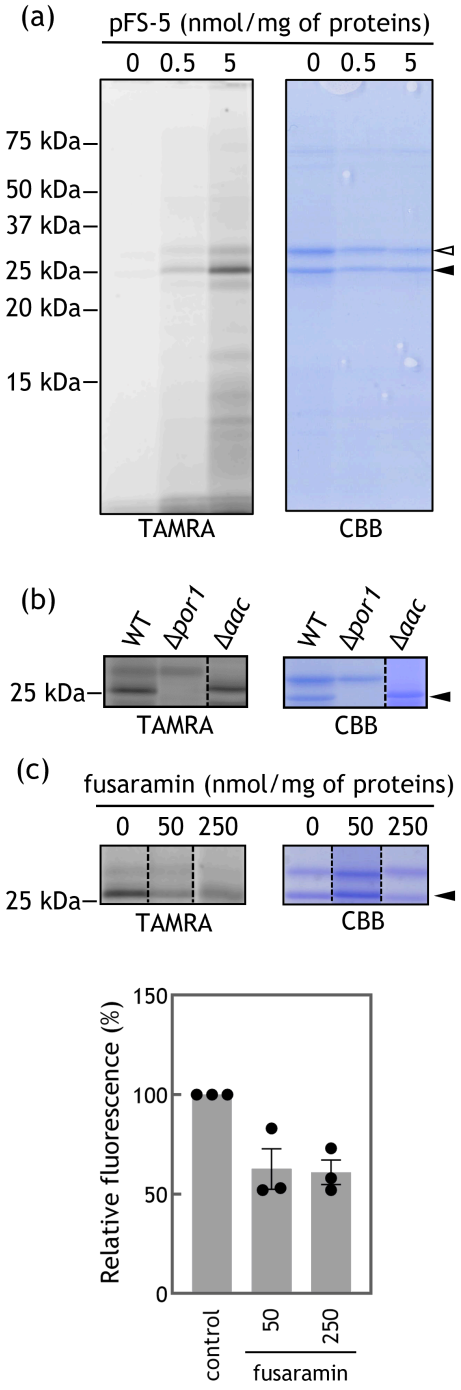
(a)
pFS-5 (nmol/mg of proteins)
0 0.5 5
0 0.5 5
75 kDa
50 kDa
37 kDa
25 kDa
20 kDa
15 kDa
TAMRA
CBB
(b)
WT
Δpor1
Δaac
25 kDa
TAMRA
CBB
(c)
fusaramin (nmol/mg of proteins)
0 50 250
0 50 250
25 kDa
TAMRA
CBB
Relative fluorescence (%)
150
100
50
0
control
50
250
fusaramin

Figure 5

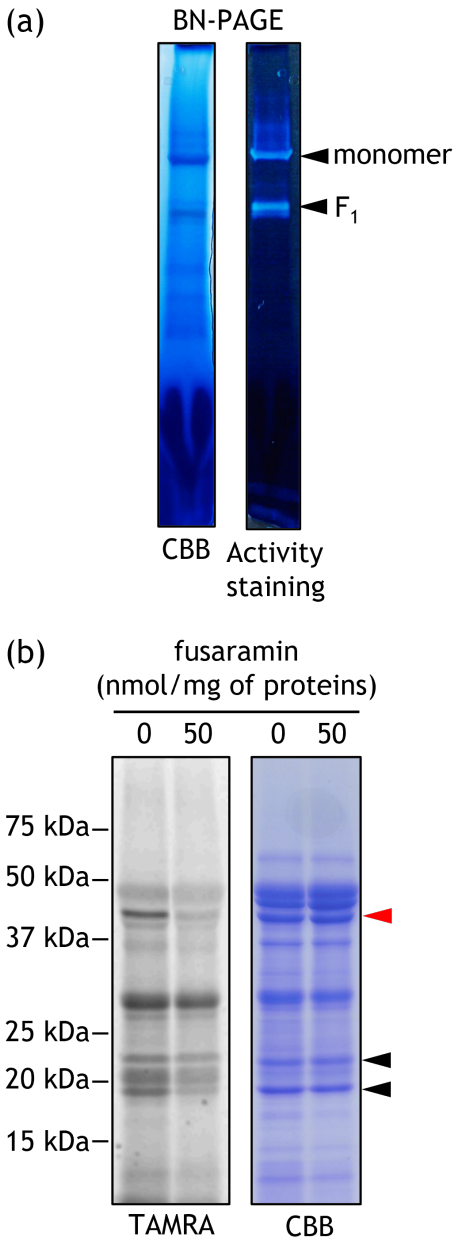
(a)
BN-PAGE
monomer
F1
CBB
Activity staining
(b)
fusaramin (nmol/mg of proteins)
0
50
0
50
75 kDa
50 kDa
37 kDa
25 kDa
20 kDa
15 kDa
TAMRA
CBB

Figure 6